Aerosol optical properties during the 2004 New England Air Quality Study–Intercontinental Transport and Chemical Transformation: Gulf of Maine surface measurements—Regional and case studies

Berko Sierau,[1] David S. Covert,[2] Derek J. Coffman,[3] Patricia K. Quinn,[3] and Timothy S. Bates[3]

[1] We report results from the 2004 New England Air Quality Study–Intercontinental Transport and Chemical Transformation (NEAQS-ITCT) based on measurements of aerosol optical properties in the marine boundary layer of the Gulf of Maine. The in situ data collected on board the NOAA research vessel *Ronald H. Brown* includes extensive properties of aerosol scattering coefficient, absorption coefficient, and optical depth at multiple wavelengths in the visible. From these, intensive properties were derived, including the Ångström exponent of scattering, single scattering albedo, and submicrometer fraction of scattering. The optical particle properties were sorted by time and location on the basis of aerosol source regions and air mass back trajectories. The results indicate a large degree of temporal and spatial variability in the observed parameters: up to 80% in the scattering and absorption coefficients, 55% in the Ångström exponent, 16% in the single scattering albedo, and 25% in the submicrometer fraction of scattering. The variability is mainly due to the multitude of aerosol sources and transport pathways in the study area. During NEAQS 2004 the mean scattering coefficients were about 20 to 40% lower than those measured during NEAQS 2002 but showed a similar variability. The mean absorption coefficient for the aerosol during NEAQS 2002 was about 80% larger than that measured during NEAQS 2004. The modal parameters of the volume-size distributions and refractive index and density of the particles were consistent with the aerosol models used in the MODIS land and ocean aerosol retrieval algorithms.

1. Introduction

[2] The 2004 NEAQS-ITCT study (F. C. Fehsenfeld et al., International Consortium for Atmospheric Research on Transport and Transformation (ICARTT): North America to Europe: Overview of the 2004 summer field study, submitted to *Journal of Geophysical Research*, 2006) was conducted in July and August 2004 in the northeastern part of the United States. The goals of the experiment were to study the urban pollution outflow from the northeastern United States, mainly from New York and Boston, and to investigate the physical and chemical evolution of the pollution plumes as they were transported from the source regions into the Gulf of Maine and along the NE U.S. coast. We present in situ data of aerosol optical properties collected on board the NOAA research vessel *Ronald H. Brown* that was deployed in the Gulf of Maine. The *Ronald H. Brown* was equipped with an array of instrumentation to characterize gaseous and particulate constituents of the air masses in the boundary layer. The ship-based measurements were coordinated with intensive space-borne and airborne measurements. The measured aerosol optical properties presented here include the scattering coefficient, σ_{sp}, and the absorption coefficient, σ_{ap}, which were determined at three wavelengths in the visible and for two particle size ranges. Several parameters were calculated from these measurements: the scattering Ångström exponent, $\mathring{a}_{scat}$, that describes the wavelength dependence of aerosol scattering and which is a measure of the aerosol particle size distribution; the single scattering albedo, ω, and the submicron fraction of scattering, SMF_{scat}.

[3] Atmospheric aerosol concentrations are significantly elevated above natural levels in regions where there is extensive urban and industrial development [e.g., *Kaufman et al.*, 2002; *Tanré et al.*, 2001; *Brock et al.*, 2003]. These

[1]Department of Atmospheric Sciences, University of Washington, Seattle, Washington, USA.
[2]Joint Institute for the Study of the Atmosphere and Ocean, University of Washington, Seattle, Washington, USA.
[3]Pacific Marine Environmental Laboratory, NOAA, Seattle, Washington, USA.
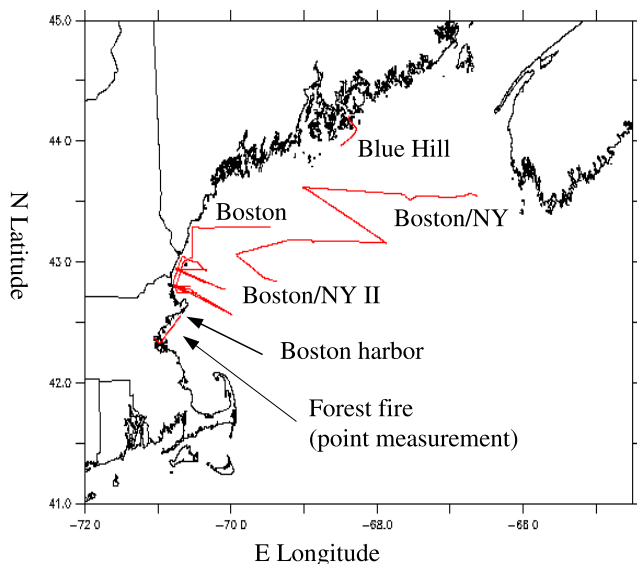
Figure 1. Area of NEAQS 2004 operation. Ship tracks of the case study as discussed in section 3.2 are labeled. The air mass from the forest fire source was measured at one ship position (42.4°N, 70.9°W) over a period of approximately 4 hours.

aerosols affect health, visibility, radiation balance and the overall chemistry of the air. They impact the radiative balance of the earth/atmosphere system directly by scattering and absorbing sunlight and indirectly by acting as cloud condensation nuclei, thereby influencing the albedo, geographical extent and life time of stratus and stratocumulus clouds and the precipitation fields associated with those clouds. Anthropogenic activities have perturbed aerosol concentrations and chemical composition over many regions of the globe which also include the east coast of the United States [*Quinn and Bates*, 2005]. Major goals of the NEAQS-ITCT 2004 field campaign were to characterize the chemical, physical and optical properties of the regional aerosol, to determine how these properties affect regional air quality, to estimate their radiative effects on climate forcing, to determine the physical and chemical transformation of aerosol emissions from the east coast during their transport and mixing downwind of the sources, as well as to characterize sources.

[4] In addition to an overview of aerosol optical properties, this paper also focuses on their regional means and variability. The spatial and temporal variability in aerosol optical properties is important for the development and improvement of chemical transport models and the determination of aerosol (radiative) properties from space. For example, the retrieval of aerosol properties using MODIS (Moderate Resolution Imaging Spectroradiometer) spectral radiances is performed using lookup tables of radiances calculated from aerosol models (including size distributions and chemical parameters) to closely match the measured radiances. These aerosol input parameters cannot be measured remotely and are based on published in situ measurements. In the retrieval algorithms these parameters are constant over large regions of the earth (e.g., only two

nondust models are used in the MODIS land algorithm over North America [*Remer et al.*, 2005]), and, therefore, uncertainties in satellite-retrieved parameters can result from synoptic and mesoscale variability in aerosol properties. We document the regional and temporal variability of aerosol optical properties, analyze relationships between chemical, physical and optical parameters and discuss them in the context of trajectories, sources and aerosol models used in the MODIS land and ocean algorithm.

[5] The data analysis and discussion in this paper are divided into three main parts.

[6] 1. A classification of the measured and derived aerosol optical properties based on the large-scale air mass trajectories. Using backward simulations of the Lagrangian particle dispersion model FLEXPART [*Stohl et al.*, 1998, 2004], time periods were selected and combined when the aerosol sampled at the ship was transported by air masses moving "offshore" or "onshore," and when the aerosol was transported from the Boston urban area. This categorizes the optical properties of the continental aerosol (offshore flow), the NW Atlantic marine aerosol (onshore flow), and the polluted urban aerosol (Boston flow), documents the variability of the regional aerosol and gives an insight into the impact of the Boston and NE U.S. plumes on the regional air quality and the aerosol radiative forcing properties.

[7] 2. Case studies of the optical properties selected according to smaller-scale features of the air masses. Six cases were identified and investigated including four urban plumes, a forest fire plume and air from a rural area in northern New England. This classification was again done utilizing FLEXPART and partly follows that of *Quinn et al.* [2006] dealing with the chemical aerosol properties measured and analyzed for these cases.

[8] 3. Finally, relationships between aerosol physics and chemistry are investigated, i.e., how the average particle chemical composition and aerosol size distribution varied with the air mass sources and/or the case study periods. The goal is to understand to what extent the optical particle properties can be explained by particle size distribution, chemical composition and refractive index. These chemical and physical aerosol properties will be presented in a way comparable to the aerosol properties used in the MODIS ocean retrieval methods [*Levy et al.*, 2003; *Remer et al.*, 2005]. The data set collected during NEAQS 2004 allows a comparison of the measured chemical, physical and optical aerosol properties to the ones assumed in the satellite algorithms. This analysis helps to assess how well the model parameters reflect realistic values of aerosol properties and how the standard deviations assumed in the aerosol models represent the temporal and spatial variability of the investigated aerosol.

2. Methods

2.1. Area and Time of Operation

[9] The NEAQS-ITCT 2004 field experiment took place in the northeastern United States in the summer of 2004. The data presented in this paper were collected on board the NOAA (National Oceanographic and Atmospheric Administration) research vessel *Ronald H. Brown* (RHB) deployed in the Gulf of Maine (Figure 1) between 5 July and 12 August.

Figure 1 also identifies the specific cruise tracks during the six case study periods.

2.2. Aerosol Inlet, Instrumentation, and Measured Quantities

2.2.1. Aerosol Sampling

[10] The sample air was drawn down a 6 m long mast through a horizontal inlet 5 cm in diameter, approximately 18 m above sea level and about halfway between the bow and the stack. The ship's heading was maintained so that the relative wind was forward of the inlet during sampling. The inlet was rotated into the relative wind to maintain nominally isokinetic flow and minimize the loss of supermicron particles. Downstream of the inlet the sample air passed through an expansion cone and a 90° bend into the sampling mast (20 cm inner diameter) at a flow of 1 m^3 min^{-1}. On the basis of *Bates et al.* [2002] particle losses in the inlet become relevant (>5%) for a particle diameter >6.5 μm. During NEAQS 2004 the mean volume diameter of the assumingly largest particles of marine origin was determined to 3.06 ± 1.77 μm (see below) and, therefore, particle losses inside the sampling mast were considered as negligible. The last 1.5 meters of the mast were heated as needed to dry the aerosol and to establish a stable reference relative humidity (RH) of 55 ± 10% for all size segregation and subsequent aerosol sampling and in situ measurements. A more detailed description of the aerosol sampling mast including its inlet efficiency is given by *Bates et al.* [2002]. Technical details are published at http://saga.pmel.noaa.gov/instrument/mast/. Before the sample air entered the optical instruments, impactors were used to remove larger particles. Submicron (sub-1) measurements were obtained by removing supermicron particles (>1 μm aerodynamic diameter) from the sample stream using a multiorifice impactor [*Berner et al.*, 1979]. Similarly, an impactor was used to remove particles larger than 10 μm for the (sub-10) micron samples.

[11] Control of size selection, sampling and measurement at an RH of ~55% followed our standardized sampling protocols and makes the data comparable to other field campaigns (e.g., ACE 1, ACE 2, INDOEX, ACE Asia, NEAQS 2002). A relative humidity of 55% was also chosen to reduce impactor bounce [*Quinn et al.*, 2002]. Dividing the measurements into sub-1 and sub-10 micron sizes follows the measurement strategy described by *Anderson et al.* [1999, 2000], and *Masonis et al.* [2002, 2003], to separate the soil and sea salt particles, mainly larger than 1 μm in diameter, from most anthropogenic aerosol, i.e., particles mainly smaller than 1 μm.

2.2.2. Aerosol Optical Properties

[12] Scattering properties were measured using two nephelometers (TSI St. Paul, MN, model 3563) [e.g., *Anderson and Ogren*, 1998]. One nephelometer measured the integral scattering and hemispheric backscattering coefficient of the sub-1 aerosol, the other that of the sub-10 aerosol. Scattering was measured at three wavelengths, 450 nm, 550 nm and 700 nm. The campaign-wide average RH of the sample flow inside the sub-1 nephelometer was 60 ± 3% (std dev), while the RH inside the sub-10 nephelometer was 52 ± 3%. Flow rates through both nephelometers were controlled at ~30 lpm. Scattering values measured by the nephelometers were corrected for angular nonidealities, including trunca-

tion errors and non-Lambertian response of the nephelometer as described by *Anderson and Ogren* [1998]. The determination of the integrated scattering uncertainty consisting of instrument noise, nephelometer accuracy, calibration uncertainty and angular truncation correction uncertainty is based on the findings by *Anderson et al.* [1996, 2003] and *Anderson and Ogren* [1998] and adjusted for scattering level and averaging time. In the second half of the first leg of the cruise, the calibration of the sub-1 nephelometer drifted because of a change in the opacity of the internal calibration shutter. The scattering data have been corrected for this drift using a correction function based on regular field recalibrations of the instrument as described by *Anderson and Ogren* [1998]. However, the additional uncertainty due to this correction could not be determined accurately and is not included in the overall uncertainty presented here.

[13] Light absorption was measured with the filter-based particle soot absorption photometer (PSAP, Radiance Research, Seattle, WA) at three wavelengths, 467 nm, 530 nm, and 660 nm [*Virkkula et al.*, 2005]. It was measured at RH < 40% to reduce the effects of RH changes on the optical path as a source of uncertainty [*Anderson et al.*, 2003]. Absorption measurements were done for the submicrometer aerosol only. The flow rate through the PSAP was ~1 lpm. Filters in the PSAP were changed before transmission values <0.6 were reached. Sources of uncertainty in the PSAP measurement include noise, drift, and correction for the scattering artifact [*Bond et al.*, 1999; *Anderson et al.*, 2003] and were adapted from the findings for the 1-λ PSAP to the 3-λ PSAP. Absorption values were corrected for the scattering artifact, the deposit spot size, instrument calibration bias, and the PSAP flow rate as described by *Bond et al.* [1999]. The nephelometer scattering data were used to make the filter-based scattering correction. The scattering values were adjusted to the PSAP wavelengths using the calculated scattering Ångström exponent as described below. This scattering correction also includes an additional $f(RH)$ correction factor because the Bond correction is based on "dry"-scattering values. The σ_{sp} values measured at ~60% RH were reduced by a factor f determined by $f(550\ nm) = \sigma_{sp}$ (~30% RH, 550 nm)/σ_{sp} (~60% RH, 550 nm). The data at ~30% RH were measured by a third, "dry" nephelometer not further discussed in this paper. Another set of calibration factors for the 3-λ instrument was reported by *Virkkula et al.* [2005]. At the relatively high single scattering albedo and low filter loadings seen in NEAQS2004, our results would be roughly 25% lower if the Virkkula scheme were used. The reasons for the discrepancy are not clear; Virkkula et al. suggest that their use of soot from a flame for calibration rather than nigrosin dye used by *Bond et al.* [1999] may be responsible. Neither particle type is representative of atmospheric aerosol. Also, the calibration soot aerosol had an ω < 0.9 and high concentration resulting in rapid filter loading and relatively low filter transmittance. The light source and optical path in the prototype instrument used by Virkkula et al. was significantly different than in the unit used in NEAQS2004. Calibration results since then with the improved optics do not support the logarithmic transform of Virkkula et al., and are closer to the algorithm of *Bond et al.* [1999] (D. S. Covert and T. C. Bond, personal

communication, 2006). Thus we believe our results to be within the stated range of uncertainty.

[14] Aerosol optical depth, AOD, was measured using three, five-channel, handheld Microtops sunphotometers (Solar Light Co., Glenside, PA; two units had wavelengths of 380, 440, 500, 675, and 870 nm, one unit had wavelengths of 340, 380, 500, 675, and 870 nm).

[15] Besides the directly measured extensive aerosol properties described above, i.e., σ_{sp}, σ_{ap}, and AOD, the following intensive properties are derived from these extensive properties. This includes the submicron fraction of scattering (SMF) at 550 nm,

$$\mathrm{SMF}_{scat} = \frac{\sigma_{sp}\left(\mathrm{D_p} < 1\mu m\right)}{\sigma_{sp}\left(\mathrm{D_p} < 10\mu m\right)} \quad (1)$$

the scattering Ångström exponent $\mathring{a}_{scat}$ from λ_1 to λ_2 for sub-1 and sub-10 micrometer measurements,

$$\mathring{a}_{scat} = -\frac{\log\left\{\sigma_{sp}(\lambda_1)/\sigma_{sp}(\lambda_2)\right\}}{\log\{\lambda_1/\lambda_2\}} \quad (2)$$

and the single scattering albedo at 467, 530, 550, and 660 nm, for sub-1 micrometer measurements

$$\omega_{sub1} = \frac{\sigma_{sp}}{\sigma_{sp} + \sigma_{ap}} \quad (3)$$

Wavelength adjustments to σ_{sp} are required to calculate ω_{sub1} because scattering and absorption coefficient were not measured at the same wavelengths (the same applies to ω presented for 550 nm). All wavelength corrections were made assuming an exponential dependence as shown in equation (2). Scattering at 467 nm was calculated using $\mathring{a}_{scat}$ of the 450/550 nm-wavelength pair, scattering at 530 nm using $\mathring{a}_{scat}$ of the 450/700 nm-wavelength pair, and scattering at 660 nm using $\mathring{a}_{scat}$ of the 550/700 nm wavelength pair. Similarly, absorption at 550 nm was calculated using $\mathring{a}$ of absorption of the 467/660 nm wavelength pair.

[16] Relative uncertainties of the presented extensive and intensive optical properties are estimated to be ±8% ($\sigma_{sp,sub1}$), ±29% ($\sigma_{sp,sub10}$), ±25% ($\sigma_{ap,sub1}$), ±14% ($\mathring{a}_{scat,sub1}$), ±55% ($\mathring{a}_{scat,sub10}$), ±7% ($\omega$), and ±30% (SMF$_{scat}$) for the given wavelengths and the 1-min time resolution. These uncertainties are applicable to the average values over the entire cruise. The scattering and absorption uncertainties are based on the 95% confidence intervals according to *Anderson et al.* [2003] and *Bond et al.* [1999]. Wavelength adjustments and RH adjustments were not considered in the overall uncertainty. The uncertainty of the Microtops is estimated to be ±0.015 AOD. Uncertainties were adjusted for different time resolution and number of averaged data points as applicable.

2.2.3. Aerosol Size Distribution and Chemical Properties

[17] The aerosol number-size distribution from 20 nm to 10 μm was measured at 60 ± 5% RH with a combination of a differential mobility particle sizer system (DMPS) and an aerodynamic particle sizer (APS 3321, TSI, St. Paul, MN). Mobility distributions were inverted to number-size distri-

butions and aerodynamic diameters were converted to geometric diameters using density derived from coarse mode chemical analysis (see *Quinn et al.* [1998, 2002] for further details). Uncertainties in the DMPS-measured size distribution include instrumental errors of particle sizing (±5%) and counting (±10%) due to flow instabilities [*Bates et al.*, 2004].

[18] The additional physical and chemical particle properties for the comparison with the MODIS aerosol model, e.g., particle density and refractive index, were determined using the aerosol chemical composition measured with a seven-stage multiorifice cascade impactor [*Berner et al.*, 1979] at 60 ± 5% RH, and a chemical thermodynamic equilibrium model to estimate the water mass associated with the relevant inorganic ions as described by *Quinn et al.* [1998], *Quinn and Coffman* [1998], and *Quinn et al.* [2002]. The organic mass was assumed to not take up any water. This assumption is supported by the results of a thermodynamic equilibrium model [*Ming and Russell*, 2002] used to estimate hygroscopic growth factors of organic-electrolyte mixtures measured in ACE-Asia RHB samples. However, neglect of the hygroscopic growth of organic aerosol components might introduce an error in the calculation of the refractive index by the method of partial molar refraction [*Stelson*, 1990] that is used herein. The relative uncertainty of the particle density and the refractive index is approximately 30% [*Quinn et al.*, 2004].

2.3. Data Processing and Presentation

[19] The results represent 1 min averages from data collected with 5 s and 1 s time resolution for the nephelometers and the PSAPs, respectively. All concentration-dependent parameters, i.e., extensive properties, are reported at standard temperature and pressure (273.2 K and 1013 mbar). The data set was cleared of fog periods, local ship traffic and short-term power plant plumes. The fog clearing is based on a calculation of water vapor saturation, S, at the time of the measurement. Periods of saturation including the uncertainty range of the RH sensor (i.e., S $\geq$ 0.98) were excluded. Fog periods were excluded from data analysis because high RH or supersaturated conditions result in large removal rates of highly hydrated aerosol locally in the foggy marine surface layer or in the aerosol sampling inlet nozzle. The data were cleared of contamination from local ship traffic and short-term power plant plumes using the trace gases SO_2, NO, NO_x, NO_y, and CO as plume markers. Starting with a running 20 min average "background" value and a threshold of 2 ppbv for SO_2, NO, NO_x, NO_y, and 30 ppbv for CO, data indicated by excursions above the background plus threshold were eliminated (E. Williams, personal communication, 2005). Furthermore, the contamination time period was extended by ±1 min to account for possible differences in the detection time due to different positions of the inlet locations (gas phase versus aerosol phase) and residence time of the sample air in the respective inlets before entering the individual sensing volumes.

[20] The determination of the submicron fraction of scattering SMF$_{scat}$ (see equation (1)) requires a measure of σ_{sp} sub-1 and σ_{sp} sub-10 at the same RH. Because the sub-1 and sub-10 nephelometers measured at two different relative humidities, on average 60% and 52% RH respectively, the

sub-1 scattering data was adjusted to the relative humidity in the sub-10 nephelometer. This was done using an $f(RH)$ correction function determined from scanning RH nephelometry data that were made on board [*Carrico et al.*, 2003; W. Wang et al., Aerosol optical properties over the northwestern Atlantic Ocean during NEAQS-ITCT 2004, submitted to *Journal of Geophysical Research*, 2006]. Scanning RH nephelometry allows the determination of the aerosol hygroscopic response in the form of a continuous function $f(RH)$ for 35% < RH < 85% that was applied to the sub-1 micron scattering data.

3. Results and Discussion

3.1. Large-Scale Air Mass Classification

[21] Aerosol optical properties were classified into three groups based on the origin of the air masses: (1) "offshore flow" class, (2) "onshore flow" class, and (3) "Boston flow" class. This classification was chosen to characterize the optical properties of the main regional-scale air masses and their sources including westerly flow bringing continental air masses into the Gulf of Maine, aerosol from the oceanic region represented by air masses coming from the east and south, and the collective polluted urban plumes coming from the Boston area. This classification characterizes the optical particle properties of the different sources and represents a measure of their large-scale variability during the period of the campaign. The entire data set of the campaign is also presented to give a campaign wide overview of the measured optical particle properties and to set their variability in context to the three main groups of different air mass origin mentioned above.

3.1.1. Classification of Air Masses

[22] Classification of the air masses into three main groups was done using the FLEXPART model [*Stohl et al.*, 1998, 2004] available for the campaign at http://www.al.noaa.gov/ICARTT/analysis/. FLEXPART uses a Lagrangian particle ("infinitesimally small parcels of air;" see *Stohl et al.* [2002]) dispersion model and cluster analysis of the air parcel positions to derive transport path and backward trajectory ensembles for the air mass of interest. It employs global meteorological input fields from ECMWF or GFS to calculate the parcel's position and time along an ensemble-averaged back trajectory. Only the ECMWF data was used in our classifications. One FLEXPART product used here ("footprint residence time") accounts for the parcel's origin and its source strength averaged over the lowest 150 m above the surface. This product gives a good indication where anthropogenic emissions have accumulated in an air mass because these emissions are mainly emitted in the planetary boundary layer.

[23] The periods selected as "offshore" were the times when the model indicated that the air masses arriving at the ship's position came from a southwesterly to northerly direction. The particle footprints originated on the continent and the air masses spent less than two days over the ocean with minimal boundary layer mixing until just prior to reaching the ship's position. The "offshore" period represents approximately 92% of the entire data set.

[24] The periods selected as "onshore" were the times when the plume trajectory and sampled air masses passed over coastal waters during the last 48 to 72 hours before reaching the ship. Prior to that time the trajectory was at altitudes of 3000 m or greater in anticyclonic flow centered over central and eastern Canada and subsided from above 3000 m to the surface in the time over water. The modeled exchange with the boundary layer was less than 30%. For a few hours during the "onshore flow" period, the model indicated that parcels from the Ohio River Valley contributed to the air mass due to shear and boundary layer mixing even though the trajectory centroid was over Canada.

[25] The periods selected for the "Boston flow" are based on FLEXPART footprint images and NO_2 source contribution as well as NO_2 concentration measured on board the RHB. This class is largely confined to air masses coming from the Boston area and the influence of other major urban sources, e.g., New York, was minor.

[26] This classification only addresses the particle properties of three main large-scale air mass groups and does not cover the entire scenario of possible air mass origins. Case studies of selected aerosol sources are discussed in section 3.2.

3.1.2. Aerosol Optical Properties

[27] The results for the cruise as a whole and for the three trajectory classifications are presented statistically as central values and variation in graphical and tabular format. Figure 2 shows the cumulative distribution functions (CDFs) for the extensive parameters $\sigma_{sp,sub1}$ (550 nm), $\sigma_{sp,sub10}$ (550 nm), $\sigma_{ap,sub1}$ (530 nm); and the intensive parameters $\mathring{a}_{scat,sub1}$, $\mathring{a}_{scat,sub10}$ for the 450/700 nm wavelength pair; the SMF_{scat} (550 nm); the ω (550 nm, sub-1); and the AOD (550 nm). The mean and median (50-percentile) values and the standard deviations ($\pm 1\sigma$) of the individual optical properties and air mass classes are summarized in Table 1.

[28] Over the entire cruise, the scattering coefficients $\sigma_{sp,sub1}$ and $\sigma_{sp,sub10}$ had mean values of 45.9 Mm^{-1} and 58.6 Mm^{-1}, respectively. The relative standard deviations of the sub-1 and sub-10 scattering were similar for both size ranges at approximately $\pm 80\%$ because of the variable nature of the sources and transport. The mean and standard deviation of $\sigma_{sp,sub1}$ and $\sigma_{sp,sub10}$ for the "offshore" class are almost identical to the respective values of the entire cruise (see Table 1). This result is similar for all optical properties analyzed in this section because the number of data points classified by air masses coming "offshore" represents approximately 92% of the entire data set (the equivalent of approximately 15 days of measurement after fog and plume clearing of the data). Note that a large fraction of the data points actually characterized by "onshore" flow were eliminated because of the fog clearing procedure. The mean values of the sub-1 and sub-10 scattering coefficient for the "Boston" class were slightly higher than the overall mean. The mean scattering values of the "onshore" class were the highest with 68.1 ± 24.7 and 98.3 ± 35.4 Mm^{-1} because of the contribution of scattering by sea salt particles and, as expected, were less variable because of the lack of proximate sources in that sector. The chemistry data, however, indicate that a time period of a few hours (finally the equivalent of approximately 1.5 hr of measurement after fog and plume clearing of the data) included in the "onshore" class was characterized by high scattering values due to non-sea-salt sulfate in the

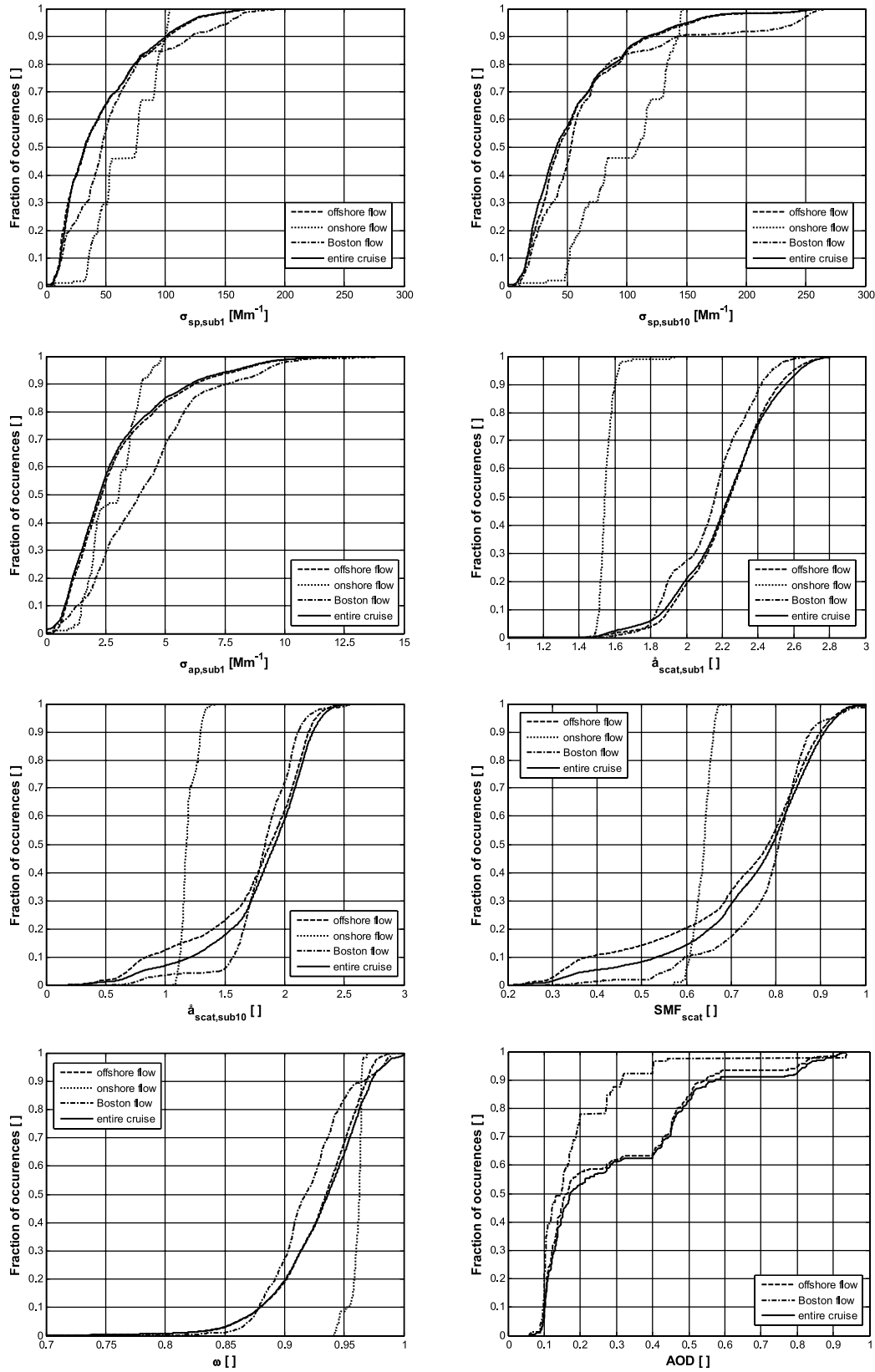**Figure 2.** Cumulative distribution functions of the aerosol optical parameters $\sigma_{sp,sub1}$, $\sigma_{sp,sub10}$, $\sigma_{ap,sub1}$, $\mathring{a}_{sp,sub1}$, $\mathring{a}_{sp,sub10}$, SMF_{scat}, ω_{sub1}, and AOD for the large-scale air mass classification.

Table 1. Aerosol Optical Properties Based on Large-Scale Air Mass Classification Using FLEXPART[a]

	$\sigma_{sp,sub1}$, Mm^{-1}	$\sigma_{sp,sub10}$, Mm^{-1}	$\sigma_{ap,sub1}$, Mm^{-1}	$\mathring{a}_{sp,sub1}$	$\mathring{a}_{sp,sub10}$	SMF$_{scat}$	ω_{sub1}	AOD
Offshore flow								
Mean	45.9	58.6	3.0	2.2	1.7	0.72	0.93	0.29
Median	32.9	43.1	2.3	2.2	1.9	0.78	0.94	0.16
Standard deviation	36.7	46.4	2.3	0.2	0.5	0.18	0.04	0.22
Onshore flow								
Mean	68.1	98.3	2.8	1.6	1.2	0.64	0.96	
Median	76.0	109.4	3.1	1.5	1.2	0.64	0.96	
Standard deviation	24.7	35.4	1.0	0.1	0.1	0.02	0.01	
Boston flow								
Mean	56.1	70.0	4.2	2.1	1.8	0.78	0.92	0.19
Median	46.9	53.1	3.9	2.2	1.8	0.81	0.92	0.15
Standard deviation	41.2	61.4	2.5	0.2	0.3	0.11	0.03	0.15
Entire cruise								
Mean	45.9	56.6	2.9	2.2	1.8	0.75	0.93	0.3
Median	32.5	41.1	2.3	2.2	1.9	0.79	0.94	0.17
Standard deviation	35.9	46.0	2.3	0.3	0.4	0.16	0.04	0.23

[a]For each classification the three rows give the mean value, median value and standard deviation ($\pm 1\sigma$). Scattering properties are given at 550 nm, absorption at 530 nm, the single scattering albedo and aerosol optical depth at 550 nm, Ångström exponents for the 450/700 nm wavelength pair.

aerosol and water uptake at 60% RH. The FLEXPART analysis leaves the source of the non-sea-salt sulfate unclear. Excluding this time period from the averaging process reduces the mean values of scattering of the "onshore" class to 55.4 ± 16.5 and 81.3 ± 25.4 Mm^{-1}. This submicrometer σ_{sp}, however, still represents a high value with respect to a marine background aerosol with minimal anthropogenic influence. *Quinn et al.* [2000], e.g., reported a $\sigma_{sp,sub1}$ (550 nm) of 4.6 ± 3.4 Mm^{-1} measured for a marine background aerosol during ACE-2 (measured at 55% RH). Our results therefore indicate that the selected "onshore" class was anthropogenically influenced and does not represent a clear marine background aerosol. Also, because of fog and plume clearing and FLEXPART classification the "onshore flow" is represented by less than 4 hours of data (~1% of entire data set) in only one continuous time period. This strongly limits the significance of this air mass class data and is most likely part of the reason for the results discussed above. However, in the following we retain the "onshore" data like it was initially classified to be consistent in the use of the FLEXPART model.

[29] Aerosol absorption was highly variable with an overall mean of $\sigma_{ap,sub1}$ = 2.9 Mm^{-1}. The "Boston flow" shows strongly elevated absorption values due to fresh particles from urban pollution sources; 10% of the $\sigma_{ap,sub1}$ values are greater than 7.5 Mm^{-1}.

[30] The scattering Ångström exponents $\mathring{a}_{sp,sub1}$ and $\mathring{a}_{sp,sub10}$ were 2.2 and 1.7 for the entire cruise. The presence of coarse mode sea salt aerosol is most likely responsible for the decrease in the sub-10 relative to the sub-1 Ångström exponent. The Ångström exponent varies with the slope or relative magnitude of the fine versus coarse modes of the aerosol size distribution so that a low exponent (å ~ <0.7) indicates a coarse mode dominated aerosol and a high exponent (å ~ >1.5) a fine mode dominated aerosol. The CDF of the Ångström exponent of the "onshore flow" is strongly shifted toward lower values indicating an increase in the coarse mode fraction most likely due to sea salt aerosol. However, $\mathring{a}_{sp,sub10}$ of 1.18 for the "onshore" class is still high with respect to the Ångström exponent of particles of clean marine air masses as reported by

Quinn et al. [1998] of −0.52 ± 17% for ACE 1 (measured in a remote, Southern Hemisphere marine area) and by *Chamaillard et al.* [2003] of 0.5 (measured in Mace Head, Ireland; note that this value is for the 500 nm/700 nm wavelength pair and for a cutoff of the sampling inlet between 2 and 8 μm depending on wind speed). This finding supports again the assumption that the "onshore flow" was partly anthropogenically influenced and that it is not representative of a true marine background aerosol.

[31] The average SMF$_{scat}$ was 0.69. Again, the CDF of the "onshore flow" stands out from the other three classes with the lowest mean value of SMF of 0.57 which supports the result of the lowest Ångström exponent due to a dominating coarse mode fraction. The variability of SMF$_{scat}$ of 5% is small.

[32] The single scattering albedo of the submicrometer aerosol at 550 nm had a mean value of 0.93 ± 0.04 for the entire cruise as well as for the "offshore" class. For the "onshore flow" the higher coarse mode sea salt scattering values dominate the submicrometer single scattering albedo together with the elevated scattering value of the non-sea-salt sulfate dominated aerosol time period discussed above, leading to a mean value of 0.96 ± 0.01. The first aspect is a consequence of the lower tail of the coarse sea salt mode extending into the submicrometric size range.

[33] Aerosol optical depth is only reported for the "offshore" and "Boston" class and the "entire cruise;" no AOD was measured during the selected "onshore" time period because of cloud cover. The AOD mean values for the cruise as a whole and the "offshore flow" of 0.30 and 0.29, respectively, are about 65% larger than the AOD measured for the "Boston" class, 0.19. Larger scattering values were obtained for the "Boston" class compared to that of the "entire cruise/offshore" class while larger AOD values were obtained for the "entire cruise/offshore" class. Clearly, surface measurements are not representative of the entire column. However, assuming uniform mixing to the top of the boundary layer for each class, this result implies that on average the mixed depth of the "Boston" class was half of that of the "offshore" class. This is consistent with the expected lesser vertical mixing of the "Boston" class air

masses compared to that of the "offshore" class. Air from the Boston source area passes over the cold Gulf of Maine waters immediately and thus vertical mixing of the emissions is limited. For the "offshore" class, the air masses additionally include sources further inland which consequently incur deeper thermal mixing.

[34] The field experiment NEAQS 2002 took place in the same region as NEAQS 2004 (U.S. eastern seaboard) and the same set of measurements were conducted on board the RHB. The extensive properties of $\sigma_{sp,sub1}$ and $\sigma_{sp,sub10}$ measured during NEAQS 2002 were reported by *Quinn and Bates* [2005] for continental flow and 55% RH as 63.3 ± 51.8 Mm^{-1} and 70.3 ± 55.1 Mm^{-1}, respectively. These values for continental flow are comparable to the mean 2004 values of the "offshore flow" category of 45.9 Mm^{-1} ± 36.7 and 58.6 ± 46.5 Mm^{-1}, respectively. The mean scattering coefficients measured during NEAQS 2002 were, therefore, about 40 to 20% higher than those measured during NEAQS 2004 but show a similar variability. The mean absorption coefficient for the sub-10 micrometer measurement was reported as 5.43 Mm^{-1} for NEAQS 2002. This value is about 80% larger than the mean sub-1 absorption coefficient obtained during NEAQS 2004. Although the absorption measurements covered two different size ranges in the two experiments, this should not affect the comparison because light absorbing aerosol constituents are mainly found in the sub-1 micrometer size range. The relative variability in σ_{ap} of approximately $\pm 80\%$ is similar for both experiments. Another comparable value reported for the NEAQS 2002 continental data set is the sub-1 single scattering albedo at 550 nm of 0.92 ± 0.05. The single scattering albedo of the NEAQS 2004 "offshore flow" is 0.93 ± 0.04, i.e., a very similar value in terms of magnitude and variability. *Delene and Ogren* [2002] report extensive and intensive aerosol properties measured on Sable Island, NS, an anthropogenically influenced marine station located on a small island $\sim$290 km southeast ($43.9°N$, $60.0°W$) of Halifax, Nova Scotia, i.e., $6-10°$ east of the NEAQS 2004 operational area. Here, historical data for the months of July and August for $\sigma_{sp,sub1}$ and $\sigma_{sp,sub10}$ were 25.18 ± 31.99 Mm^{-1} and 50.53 ± 45.57 Mm^{-1}, $\sigma_{ap,sub1}$ was 1.98 ± 2.08 Mm^{-1}, $\mathring{a}_{sp,sub1}$ and $\mathring{a}_{sp,sub10}$ were 2.43 ± 0.40 and 1.20 ± 0.67, and ω was 0.92 ± 0.06 (average over July and August; Personal communication Elisabeth Andrews). The data were obtained at a measurement RH < 40%, therefore only a direct comparison of the absorption coefficient and the scattering Ångström exponents is reasonable because the other parameters are strongly relative humidity−dependent. *McInnes et al.* [1998] examined the hygroscopic growth factor of $\sigma_{sp,sub10}$ at Sable Island. On the basis of their findings we applied a rough $f(60\% RH/40\% RH)$ conversion factor of 1.2 to make the sub-10 scattering data comparable. The mean value of $\sigma_{sp,sub10}$ for Sable Island adjusted to 60% RH was about 60 Mm^{-1} which is at the lower end of the range measured during NEAQS 2004. The 2-month mean absorption coefficient measured on Sable Island is similar to that of the "onshore" class discussed in this section, indicating clean marine aerosol with a low fraction of absorbing components. The sub-1 scattering Ångström exponent of 2.43 ± 0.40 measured on Sable Island, however, is more comparable to the one measured for the "offshore flow," i.e., the continental influenced

aerosol, whereas the sub-10 scattering Ångström exponent of 1.20 ± 0.67 is again similar to the one measured for the "onshore" class.

3.2. Case Studies

[35] The optical particle properties were sorted by time and location on the basis of different aerosol sources [see also *Quinn et al.*, 2006]. This was done by (1) eliminating periods of marine air by applying a minimum threshold of sub-1 scattering (50 Mm^{-1}) and (2) using a combination of the FLEXPART model and chemical information to identify the air mass source (measurements of VOCs (volatile organic compounds), NO$_x$, and SO$_2$ were used as tracers of sources (urban, power plant, biogenic)). The cases selected and investigated were (1) a distant forest fire source, (2) a Boston/New York plume, (3) a Boston plume, (4) rural Blue Hill Bay near Acadia National Park, (5) Boston harbor, and (6) a second Boston/New York plume (see Figure 1). The "Boston harbor" case was not cleared of contamination from local plumes in contrast to the other cases. The short-term urban and ship plumes measured in/and or in the area of the Boston harbor represented major features of this air mass because of the sampling close to the source. Thus the plume screening procedure applied to the rest of the NEAQS 2004 data was judged to be inappropriate.

[36] The CDFs of the optical properties for the six different cases are shown in Figure 3. The variation of the case average intensive optical properties, i.e., aerosol scattering and absorption coefficients, range from 15 Mm^{-1} to 108 Mm^{-1} ($\sigma_{sp,sub1}$), 17 Mm^{-1} to 138 Mm^{-1} ($\sigma_{sp,sub10}$), and 1.7 Mm^{-1} to 9.3 Mm^{-1} ($\sigma_{ap,sub1}$), respectively. Scattering was the lowest in the Boston harbor area (15.27 ± 3.08 Mm^{-1}; sub-1; see Table 2) whereas absorption was relatively high and strongly variable (6.03 ± 4.28 Mm^{-1}) because of frequent plumes of absorbing particles coming from urban sources. The forest fire case stands out with the smallest submicrometer fraction of scattering (mean of 0.64 ± 0.01), the lowest scattering Ångström (mean of 1.17 ± 0.02; sub-10) but still a high single scattering albedo (>0.95). This is due to the comparatively large fraction of coarse mode particles (see particle surface distribution in Figure 4) and the shift of the accumulation mode to larger particle sizes during the long transport time.

[37] As previously discussed, the aerosol optical properties in or close to Boston harbor were affected by light absorption (compare $\sigma_{ap,sub1}$ of "Boston harbor" and "Boston plume" case in Figure 3) due to fresh particles from urban pollution. However, with increasing distance from the source the high absorption to scattering ratio in the air masses was not maintained as shown by the increase of the median single scattering albedo from 0.7 to values greater than 0.9 for all of the "pollution plumes." This is presumably due to physical and chemical transformation of the particles (e.g., water uptake, production of nonabsorbing aerosol mass from gas-phase reactions) and mixing/dilution with other air masses. The variability of ω of the "Boston harbor" case was 15%, 15 times higher than that of the other five cases (1−2%). This result is partly biased by using an "uncleared" data set (see above) in the "Boston harbor" case that includes highly variable absorption values due to short-term urban pollution plumes.
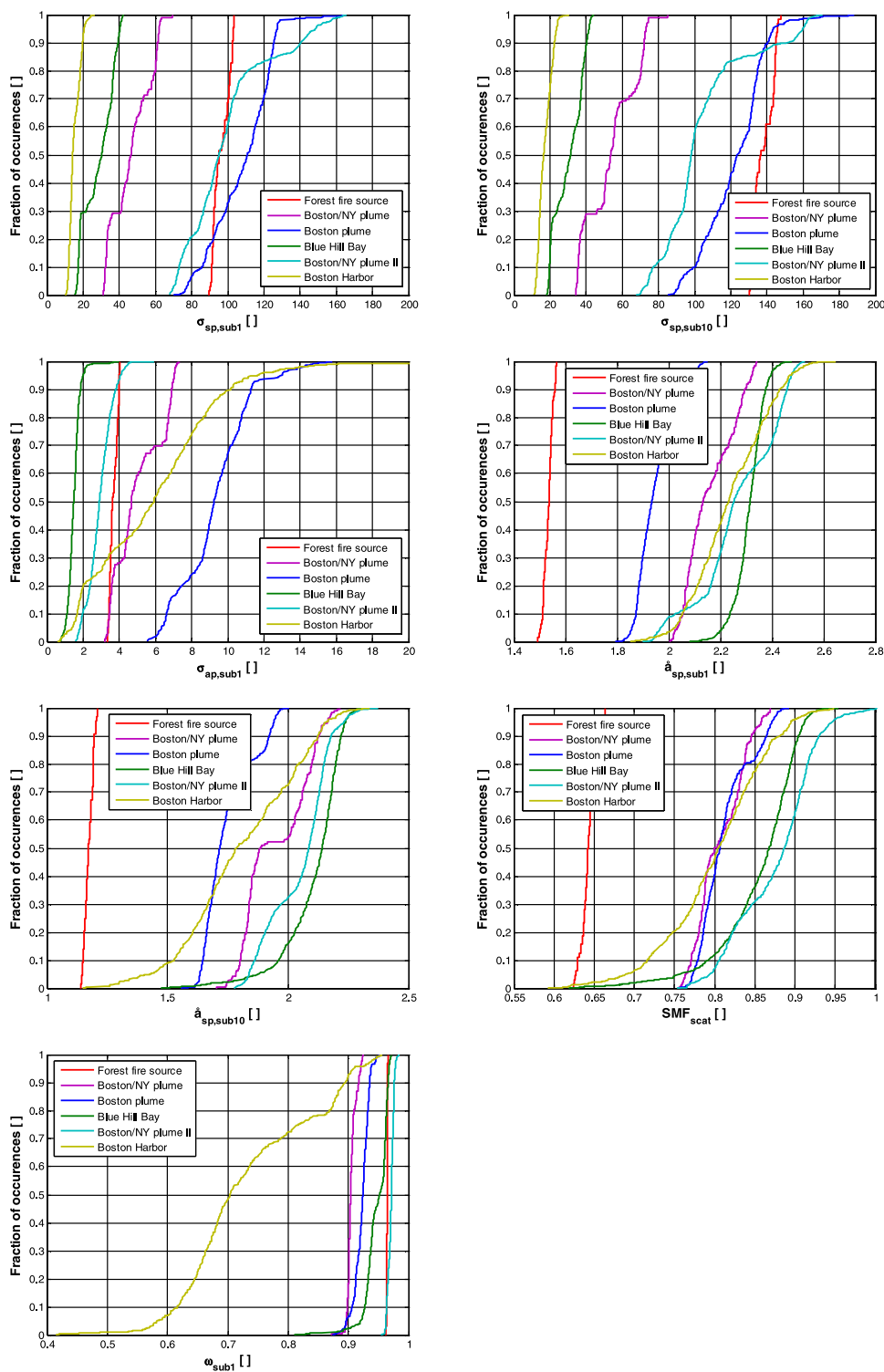
Figure 3. Cumulative distribution functions of the optical parameters for the case studies. The different cases are denoted by colors in each panel.

3.3. Variability and Consistency of Measured Physical, Chemical, and Optical Aerosol Properties and Their Relation to MODIS Aerosol Retrieval Algorithms

[38] In this section, the variability and consistency of the geometric volume mean diameter D_{gv} and the geometric standard deviation σ_g of the lognormal volume-size distribution are analyzed and discussed together with the refractive index R of the measured particles and their density ρ, g/cm^3. These size distribution parameters and chemical properties are presented in a format similar to those of the aerosol models used in the MODIS land and ocean retrievals with the goal of providing information in the context of the aerosol climatology used as basis of the retrieval algorithms.

Table 2. Mean, Median, and Standard Deviation of Aerosol Optical Properties for the Six Case Studies[a]

	$\sigma_{sp,sub1}$, Mm^{-1}	$\sigma_{sp,sub10}$, Mm^{-1}	$\sigma_{ap,sub1}$, Mm^{-1}	$\mathring{a}_{sp,sub1}$	$\mathring{a}_{sp,sub10}$	FMF$_{scat}$	ω_{sub1}
Forest fire source							
Mean	96.5	137.9	3.7	1.5	1.2	0.64	0.96
Median	95.3	136.3	3.6	1.5	1.2	0.64	0.96
Standard deviation	4.5	5.7	0.2	0.0	0.0	0.01	0
Boston/NY plume							
Mean	46.6	53.8	5.0	2.2	2.0	0.81	0.91
Median	46.7	53.7	4.7	2.1	1.9	0.8	0.9
Standard deviation	10.9	13.8	1.3	0.1	1.1	0.03	0.01
Boston plume							
Mean	108.0	122.2	9.3	2.0	1.8	0.81	0.92
Median	110.8	123.8	9.3	1.9	1.7	0.81	0.92
Standard deviation	16.3	16.7	1.9	0.1	0.1	0.03	0.01
Blue Hill Bay							
Mean	28.6	30.4	1.5	2.3	2.1	0.86	0.95
Median	30.3	31.4	1.5	2.3	2.1	0.87	0.95
Standard deviation	8.5	7.9	0.4	0.1	0.1	0.05	0.02
Boston/NY plume II							
Mean	99.5	104.2	2.9	2.3	2.1	0.88	0.97
Median	95.1	98.2	2.9	2.3	2.1	0.89	0.97
Standard deviation	23.0	23.8	0.7	0.2	0.1	0.05	0.01
Boston Harbor							
Mean	15.3	17.2	6.0	2.2	1.8	0.8	0.73
Median	14.2	16.5	5.9	2.2	1.8	0.8	0.7
Standard deviation	3.1	3.7	4.3	0.1	0.2	0.06	0.11

[a]Statistical and optical properties are given as in Table 1.

3.3.1. Size Distribution Parameters, Refractive Index, and Particle Density

[39] For the MODIS comparison the volume-size distribution parameters, refractive indices and particle densities were calculated and evaluated for the time periods and case studies discussed in sections 3.1 and 3.2. The number distributions with 5 min time resolution were again cleared of contamination from local ship traffic and short-term power plant plumes and averaged over a 1 hour time period. The resulting number distributions were converted to surface area distributions and fitted using three lognormal modes (i.e., nominally an Aitken ($\sim$0.01–0.1 μm), accumulation ($\sim$0.1–1 μm) and coarse mode ($\sim$1–10 μm) yielding the surface geometric mean diameter D_{gs} and standard deviation σ_g for each of the three lognormal modes. The surface moment was chosen for fitting because it most nearly represents the scattering distribution yet clearly illustrates the trimodal feature. Surface distribution parameters were then converted to volume-size distribution parameters for comparison to MODIS aerosol model parameters. In many cases the smallest mode was clearly in the Aitken range in terms of number mean diameter but larger than 100 nm in terms of surface mean diameter. When the smallest mode was significant in terms of separation from the accumulation mode and in terms of fractional surface area it was kept as a separate mode and termed accumulation mode 1 for consistency with MODIS terminology. The surface distributions resulting from the fitting for the case studies are shown in Figure 4, primarily as examples to show the modal structure and range of variability.

[40] The particulate refractive index R and density ρ were determined from filter analysis as described above. Typical filter sampling times were $\sim$4 to 5 hours during the day and $\sim$12 hours during the night. The size distributions measured during each filter sampling period were assigned the same value of R and ρ; no interpolation of R and ρ was done

between filter samples. The 1 hour size distributions were considered valid when greater than 50% of the 5 min size and chemical data were present after the standard screening for ship and power plant plumes (see section 2.3). The threshold of 50% was arbitrarily chosen but it ensured a relevant number of distributions for each air mass class; the occurrence of one plume event during a filter sample could contaminate the sample and overwhelm the refractive index and density data for the entire 4–12 hour time period. A strict application of the standard data clearing for ship and power plant plumes would lead to a rejection of the chemical and size distribution data for the sample. However, when allowing 50% "bad" data points for the 1 hour average period of the size distribution data a "contamination" of the filter sample, i.e., perturbed values of R and ρ, is still feasible. The 50% criterion only diminishes the probability of a nonrepresentative value of R and ρ due to the partial inclusion of short-term plume data in the averaging process.

[41] The top section of Table 3 summarizes D_{gv} and σ_g, of the accumulation and the coarse mode from the fit parameters along with their refractive indices R and densities ρ. The data are presented for the entire cruise, the air mass trajectory classes (compare 3.1) and one case study (compare 3.2) when adequate size distribution and chemical data were available to constitute a representative sample. Except for Blue Hill Bay, the case studies forest fire, Boston Harbor and both New York/Boston plumes are not listed. They are subsets of the larger classes, one-time events, or localized and not necessarily representative or comparable to the MODIS algorithm. The mean values of the parameters were obtained by averaging the respective 1 hour size distributions and chemical parameters over the time periods of the individual classes/case. Since the "entire cruise," "offshore flow" and "Boston flow" classes represent similar air mass origins, the size parameters and the chemical parameters are
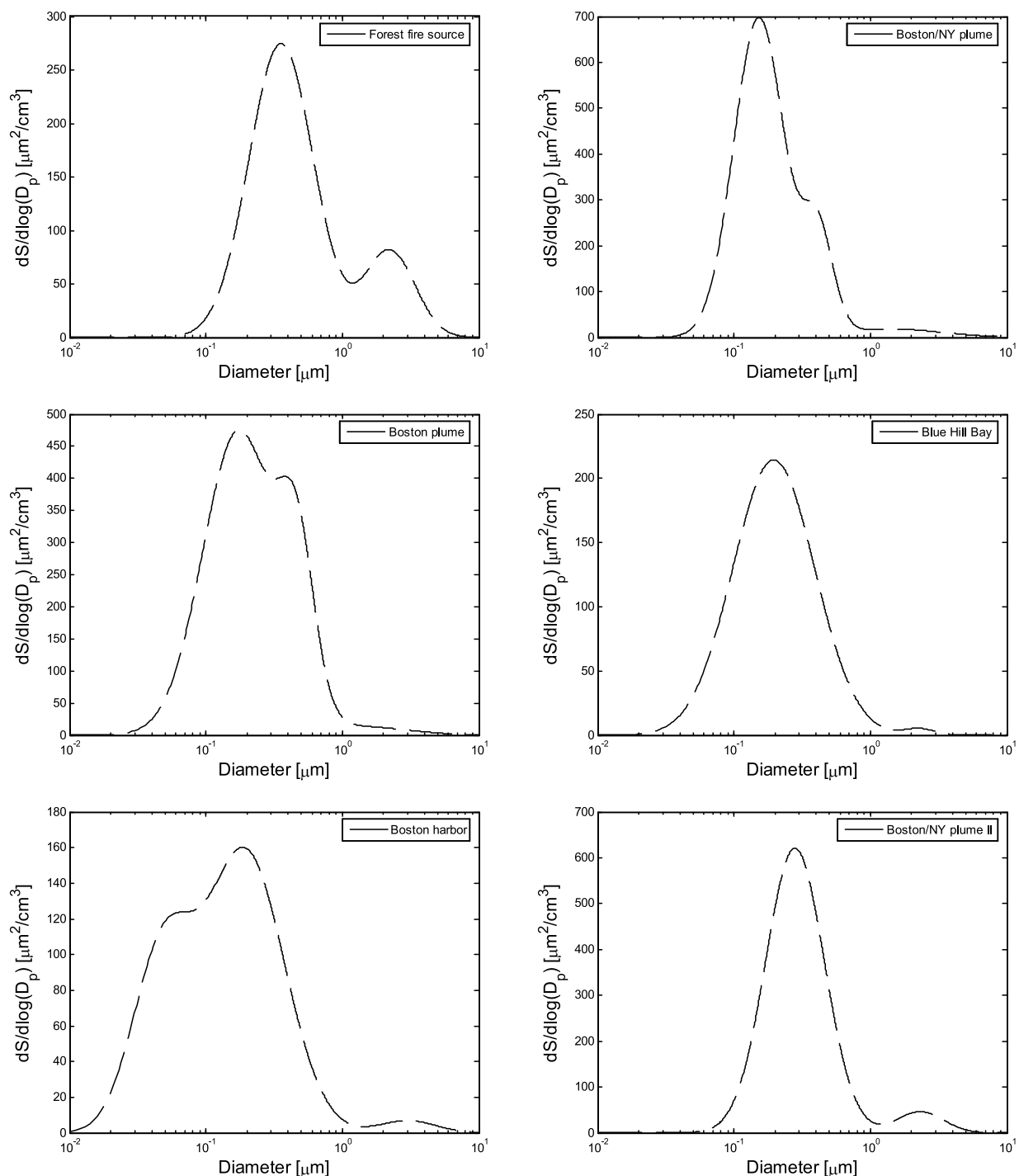
Figure 4. Surface area size distributions for the case studies. The different cases are marked in the legends.

similar, $D_{gv} = 0.19 \pm 0.01$, $\sigma_g = 1.72 \pm 0.02$, R = 1.49–0.0058i $\pm$ 0.0007i, $\rho = 1.41 \pm 0.01$. However, the "Boston flow" accumulation mode shows the largest imaginary part in its refractive index (0.0072i) which is consistent with the largest absorption coefficient and the contribution of internal combustion sources (compare Tables 1 and 2). The largest coarse mode, mean volume diameter was obtained for the "onshore flow" class. This again reflects the influence of sea salt particles on its size distribution as

already supported by the overall smallest sub-10 scattering-Ångström exponent (with exception of the forest fire case). The Blue Hill Bay case is included because it represents a different source area according to the FLEXPART and chemical analysis. The FLEXPART back trajectory footprint and CO source contribution showed the majority of the source area to be within one day transport time over Maine and NE Canada from the region of Quebec, Montreal and further toward James Bay. Over this transport time and

Table 3. Measured Aerosol Properties During NEAQS 2004 for the Classified Air Masses as Discussed in Section 3 and Properties of Aerosol Models Used in MODIS Ocean and Land Retrieval[a]

NEAQS Case/Class	Mode	Dgv, μm	σ_g	R	ρ, g/cc
Entire cruise	accumulation mode 1	0.19	1.70	1.49 − 0.0051i	1.41
Entire cruise	2	0.38	1.52	1.49 − 0.0051i	1.41
Entire cruise	coarse mode	2.87	1.67	1.47 − 0.0037i	1.58
Offshore flow class	accumulation mode 1	0.19	1.75	1.49 − 0.0053i	1.40
Offshore flow class	2	0.41	1.49	1.49 − 0.0053i	1.40
Offshore flow class	coarse mode	2.85	1.60	1.47 − 0.0034i	1.55
Boston flow class	accumulation mode 1	0.18	1.71	1.49 − 0.0072i	1.41
Boston flow class	2	0.38	1.51	1.49 − 0.0072i	1.41
Boston flow class	coarse mode	2.84	1.62	1.47 − 0.0035i	1.60
Onshore flow class	accumulation mode 1	0.26	1.67	1.51 − 0.0032i	1.42
Onshore flow class	2	0.49	1.35	1.51 − 0.0032i	1.42
Onshore flow class	coarse mode	3.06	1.77	1.45 − 0.0000i	1.41
Blue Hill Bay case	accumulation mode 1	0.17	1.66	1.49 − 0.0000i	1.41
Blue Hill Bay case	2	0.34	1.61	1.49 − 0.0000i	1.41
Blue Hill Bay case	coarse mode	2.32	1.46	1.50 − 0.0000i	1.88

MODIS Algorithm/Model	Mode	Dgv,[b] μm	σ_g[b]	R	ρ,[b] g/cc
Land algorithm	accumulation mode 1	0.212	1.82	1.43 − 0.0035i	
Urban/industrial model	2	0.42	1.57	1.43 − 0.0035i	
Urban/industrial model	coarse mode 3	2.6	1.35	1.43 − 0.0035i	
Urban/industrial model	4	19	2.56	1.43 − 0.0035i	
Ocean algorithm	accumulation mode 1	0.23	1.49	1.45 − 0.0035i	1.79
Ocean algorithm	2	0.35	1.82	1.45 − 0.0035i	1.79
Ocean algorithm	3	0.47	1.82	1.40 − 0.0020i	1.39
Ocean algorithm	4	0.59	1.82	1.40 − 0.0020i	1.39
Ocean algorithm	coarse mode 5	2.36	1.82	1.45 − 0.0035i	1.24
Ocean algorithm	6	3.53	1.82	1.45 − 0.0035i	1.24
Ocean algorithm	7	4.71	1.82	1.45 − 0.0035i	1.24
Ocean algorithm	8	3.53	1.82	1.53 − 0.0010i	2.60
Ocean algorithm	9	6.82	2.23	1.53 − 0.0010i	2.60

[a]From *Remer et al.* [2005], *Kaufman et al.* [1997], and *Anderson et al.* [2005].
[b]Taken from *Anderson et al.* [2005] except for properties of land algorithm.

distance the air arriving at the ship was a mixture of both boundary layer and free troposphere parcels. The accumulation mode diameters were smaller but not significantly compared to the other classes. The chemical analysis and scattering model showed an insignificant imaginary refractive index. The absorption coefficient $\sigma_{ap,sub1} = 1.5$ Mm^{-1} was low. However, scattering was also low and the intensive parameters, Ångström exponent and single scattering albedo, were in the range of the continental classes.

3.3.2. Size Distribution and Chemical Parameters Used in MODIS Aerosol Models

[42] The bottom section of Table 3 shows a compilation of aerosol parameters of lognormal size distributions used to generate the MODIS lookup tables for the land and ocean algorithms to retrieve aerosol optical depth and thus derive aerosol properties from satellite radiance measurements. The MODIS algorithms derive aerosol properties by comparing measured radiances to calculated radiances for the known viewing geometry and for specific values of surface reflectivity, aerosol type, and aerosol amount. A finite number of aerosol types are considered, each of which has a specific, lognormal size distribution and refractive index. The optical properties (most importantly the scattering phase function and the single scattering albedo) of each aerosol type are calculated from Mie theory and these properties are used in a large set of radiative transfer calculations to generate lookup tables for the retrieval algorithms (for a more detailed description of the MODIS algorithms see, e.g., *Remer et al.* [2005], *Kaufman et al.*

[1997], *Levy et al.* [2003], *Tanré et al.* [1997]). The land algorithm distinguishes between dust and nondust and uses a prescribed combination of coarse- and fine-mode aerosol assigned to geographical locations as basis for the radiance calculations whereas the ocean algorithm generates a solution out of possible combinations of 4 fine mode and 5 coarse mode aerosol types. Table 3 lists the size distribution parameters, refractive indices and densities of the urban/industrial nondust aerosol model which is used in the land algorithm and is assigned to the NEAQS 2004 measurement region [*Remer et al.*, 2005; *Kaufman et al.*, 1997] and the respective parameters of the 9 aerosol types/modes used in the ocean retrieval [*Remer et al.*, 2005; *Anderson et al.*, 2005]. Note that the MODIS land algorithm applies the urban/industrial model for the entire eastern United States, Canada and Greenland.

[43] In general, the size distribution parameters used in the MODIS land and ocean algorithms are consistent with our observations during NEAQS 2004. The size distribution parameters D_{gv} and σ_g of the accumulation mode used in the land and ocean algorithms are all within ±2σ of those of the accumulation mode obtained from the "entire cruise" data (2σ = ±0.18 for D_{gv} and ±0.44 for σ_g). The same applies for the ocean algorithm's coarse mode aerosol models 5 and 6 and the coarse mode 3 of the urban/industrial model which are within ±2σ of those of the coarse mode obtained from the data (±1.36 for D_{gv} and ±0.78 for σ_g). The size parameters of the coarse mode 4 of the urban/industrial model deviate further from the findings

of NEAQS 2004. Coarse mode 7 of the ocean algorithm shows also a slightly higher D_{gv} of 4.71 with respect to the $\pm 2\sigma$ standard deviation. The modes 8 and 9 are specified as "dustlike types" [*Remer et al.*, 2005] of aerosols and do not apply to our location and conditions (note that the MODIS ocean algorithm retrieves the final aerosol parameters on the basis of a combination of the 4 fine and 5 coarse mode models and is, therefore, more "flexible" in terms of its solution compared to the land algorithm). In more detail, the accumulation mode size parameters of $D_{gv} = 0.41$ μm and $\sigma_g = 1.49$ of the "offshore flow" class are very comparable to the respective values of the second accumulation mode of the urban/industrial model of $D_{gv} = 0.42$ μm and $\sigma_g = 1.57$. Although the NEAQS data were collected in the marine boundary layer the comparison to the land model is still reasonable as the "offshore flow" class data mainly represents properties of NE U.S. continental air masses. The coarse mode data show a similarity between the measured size parameters (2.85 and 1.60 for D_{gv} and σ_g, respectively) and the first coarse mode of the urban industrial model (2.60 and 1.35). The size parameters of the "onshore flow" class are within the range of the different accumulation and coarse mode aerosol models of the ocean algorithm.

[44] The mean and twice the standard deviation of the refractive index of the accumulation and coarse mode of the entire cruise yield $1.49(\pm 0.03) - 0.0051i(\pm 0.0068i)$ and $1.47(\pm 0.06) - 0.0037i(\pm 0.0174i)$ respectively. Here, the real part used in the MODIS aerosol models is found to be outside of the range of the 95% confidence interval whereas the imaginary part is within the interval. The range of MODIS accumulation mode densities of $1.39 - 1.79$ is consistent with the NEAQS "entire cruise" value of 1.41 ± 0.08 especially when considering the RH differences. Note that the particle densities reported by *Anderson et al.* [2005] and summarized here for the MODIS models represent dry densities whereas the one listed for the NEAQS data are reported for 55% RH.

[45] The single scattering albedo was also determined for the individual MODIS aerosol models but is not listed in Table 3 [see, e.g., *Anderson et al.*, 2005; *Remer et al.*, 2005]. The single scattering albedo of the two accumulation modes of the nondust urban/industrial model is reported as 0.96 and 0.97 (between $\lambda = 470$ nm and 660 nm). Those of the ocean models ($\lambda = 550$ nm) span a range between 0.97 (fine mode 1) and 0.99 (fine mode 4). The NEAQS values of the single scattering albedo were ω_{sub1} 0.93 ± 0.04 for the "offshore" flow class representing continental aerosol and 0.96 ± 0.01 for the "onshore" flow class representing more marine aerosol (compare Table 1). Thus the differences between continental and marine are consistent for MODIS and NEAQS but the NEAQS values are lower than the MODIS models by 0.03. However, the NEAQS data are reported for 55 to 60% RH whereas MODIS applies the aerosol parameters to the entire vertical column, i.e., normally for vertically integrated, higher "ambient" RH which would be consistent with a somewhat larger value of the single scattering albedo.

4. Summary and Conclusions

[46] Measurements of aerosol optical properties made on board the research vessel *Ronald H. Brown* during the 2004

NEAQS-ITCT campaign indicated a large degree of variability in the observed parameters in the study area. The large degree of variability is mainly due to the variable nature of the aerosol sources and transport in this region as shown by a classification of the air mass trajectories and case studies of specific aerosol sources. The Gulf of Maine is strongly influenced by continental sources with elevated absorption coefficients and lower single scattering albedo obtained for offshore flow or urban plumes compared to the marine or cleaner continental background aerosol. Measurements in the vicinity of the Boston harbor and data from distinct pollution plumes coming from the Boston urban area showed mean absorption values up to six times greater than the continental background value. However, with increasing distance from the sources the air masses typically did not maintain their absorption to scattering characteristics. This is seen in the increase of the single scattering albedo with increasing source distance which is presumably due to condensation of nonabsorbing mass on the particles and mixing with other air masses. A more detailed analysis of the individual urban plume cases including extensive meteorology and chemical data will give insight into physical and chemical transformation of aerosol emissions from the east coast of the United States and will be a topic of an additional paper.

[47] A comparison of the results of the NEAQS 2004 and NEAQS 2002 field campaigns showed a similar degree in the variability of the aerosol optical properties. The absolute values of the absorption and scattering coefficients of the continental air masses were about 80% and 20 to 40% higher during the NEAQS 2002 measurement period, respectively, but were still in the range of the 95% variability intervals of the NEAQS 2004 data.

[48] The values of the measured geometric volume mean diameter and the geometric standard deviation of the derived lognormal volume-size distributions, the refractive index of the measured particles and their density were generally consistent with the aerosol models used in the MODIS land and ocean aerosol retrieval algorithms. The size distribution parameters D_{gv} and σ_g of the accumulation mode used in the MODIS algorithms are all within $\pm 2\sigma$ of those of the accumulation mode obtained from the "entire cruise" data ($2\sigma = \pm 0.18$ for D_{gv} and ± 0.44 for σ_g). This was true for most of the ocean algorithm's coarse mode aerosol and the urban/industrial model of the land algorithm. While these differences in distribution values are small the effects of such differences on look-up table radiances may be larger. However, the real part of the refractive index used in the MODIS aerosol models is found to be outside of the range of the 95% variability interval of the NEAQS observations whereas the imaginary part is within the interval. The MODIS accumulation mode densities are larger than the NEAQS "entire cruise" value. In terms of the single scattering albedo the NEAQS data generally yield lower values compared to the ones of the accumulation mode of the nondust urban/industrial model.

[49] The large degree of regional and temporal variability of the optical and size distribution parameters obtained for the investigated air masses during NEAQS 2004 illustrates the necessity of quantifying aerosol properties on a regional scale. The existing variability is likely not fully reflected by the aerosol input parameters of the MODIS land and ocean

algorithm indicating that uncertainties in satellite-retrieved parameters can result from synoptic and mesoscale variability in actual aerosol properties. The findings concerning the means and variability in aerosol optical properties can also be used for the development and improvement of chemical transport models.

References

Anderson, T. L., and J. A. Ogren (1998), Determining aerosol radiative properties using the TSI 3563 integrating nephelometer, *Aerosol Sci. Technol.*, *29*, 57–69.

Anderson, T. L., et al. (1996), Performance characteristics of a high-sensitivity, three-wavelength, total scatter/backscatter nephelometer, *J. Atmos. Oceanic Technol.*, *13*, 967–986.

Anderson, T. L., D. S. Covert, J. D. Wheeler, J. M. Harris, K. D. Perry, B. E. Trost, D. J. Jaffe, and J. A. Ogren (1999), Aerosol backscatter fraction and single scattering albedo: Measured values and uncertainties at a coastal station in the Pacific Northwest, *J. Geophys. Res.*, *104*(D21), 26,793–26,807.

Anderson, T. L., S. J. Masonis, D. S. Covert, R. J. Charlson, and M. J. Rood (2000), In situ measurement of the aerosol extinction-to-backscatter ratio at a polluted, continental site, *J. Geophys. Res.*, *105*, 26,793–26,807.

Anderson, T. L., S. J. Masonis, D. S. Covert, N. C. Ahlquist, S. G. Howell, A. D. Clarke, and C. S. McNaughton (2003), Variability of aerosol optical properties derived from in situ aircraft measurements during ACE-Asia, *J. Geophys. Res.*, *108*(D23), 8647, doi:10.1029/2002JD003247.

Anderson, T. L., Y. Wu, D. A. Chu, B. Schmid, J. Redemann, and O. Dubovik (2005), Testing the MODIS satellite retrieval of aerosol fine-mode fraction, *J. Geophys. Res.*, *110*, D18204, doi:10.1029/2005JD005978.

Bates, T. M., et al. (2004), Marine boundary layer dust and pollutant transport associated with the passage of a frontal system over eastern Asia, *J. Geophys. Res.*, *109*, D19S19, doi:10.1029/2003JD004094.

Bates, T. S., D. J. Coffman, D. S. Covert, and P. K. Quinn (2002), Regional marine boundary layer aerosol size distributions in the Indian, Atlantic, and Pacific Oceans: A comparison of INDOEX measurements with ACE-1, ACE-2, and Aerosols99, *J. Geophys. Res.*, *107*(D19), 8026, doi:10.1029/2001JD001174.

Berner, A., C. H. Lurzer, F. Pohl, O. Preining, and P. Wagner (1979), The size distribution of the urban aerosol in Vienna, *Sci. Total Environ.*, *13*, 245–261.

Bond, T. C., T. L. Anderson, and D. Campbell (1999), Calibration and intercomparison of filter-based measurements of visible light absorption by aerosols, *Aerosol Sci. Technol.*, *30*, 582–600.

Brock, C. A., et al. (2003), Particle growth in urban and industrial plumes in Texas, *J. Geophys. Res.*, *108*(D3), 4111, doi:10.1029/2002JD002746.

Carrico, C. M., P. Kus, M. J. Rood, P. K. Quinn, and T. S. Bates (2003), Mixtures of pollution, dust, sea salt, and volcanic aerosol during ACE-Asia: Radiative properties as a function of relative humidity, *J. Geophys. Res.*, *108*(D23), 8650, doi:10.1029/2003JD003405.

Chamaillard, K., S. G. Jennings, C. Kleefeld, D. Ceburnis, and Y. J. Yoon (2003), Light backscattering and scattering by nonspherical sea-salt aerosols, *J. Quant. Spectrosc. Radiat. Transfer*, *79–80*, 577–597.

Delene, D. J., and J. A. Ogren (2002), Variability of aerosol optical properties at four North American surface monitoring sites, *J. Atmos. Sci.*, *59*, 1135–1150.

Kaufman, Y. J., D. Tanré, L. A. Remer, E. F. Vermote, A. Chu, and B. N. Holben (1997), Operational remote sensing of tropospheric aerosol over land from EOS moderate resolution imaging spectroradiometer, *J. Geophys. Res.*, *102*(D14), 17,051–17,067.

Kaufman, Y. J., D. Tanré, and O. Boucher (2002), A satellite view of aerosols in the climate system, *Nature*, *419*, 215–223.

Levy, R. C., L. A. Remer, D. Tanré, Y. J. Kaufman, C. Ichoku, B. N. Holben, J. M. Livingston, P. B. Russell, and H. Maring (2003), Evaluation of the Moderate-Resolution Imaging Spectroradiometer (MODIS) retrievals of dust aerosol over the ocean during PRIDE, *J. Geophys. Res.*, *108*(D19), 8594, doi:10.1029/2002JD002460.

Masonis, S. J., K. Franke, A. Ansmann, D. Müller, D. Althausen, J. Ogren, A. Jefferson, and P. Sheridan (2002), An intercomparison of aerosol light extinction and 180° backscatter as derived using in situ measurements and Raman lidar during the INDOEX field campaign, *J. Geophys. Res.*, *107*(D19), 8014, doi:10.1029/2000JD000035.

Masonis, S. J., T. L. Anderson, D. S. Covert, V. Kapustin, A. D. Clarke, S. Howell, and K. Moore (2003), A study of the extinction-to-backscatter ratio of marine aerosol during the shoreline environment aerosol study, *J. Atmos. Oceanic Technol.*, *20*(10), 1388–1402.

McInnes, L., M. Bergin, J. Ogren, and S. Schwartz (1998), Apportionment of light scattering and hygroscopic growth to aerosol composition, *Geophys. Res. Lett.*, *25*(4), 513–516.

Ming, Y., and L. M. Russell (2002), Thermodynamic equilibrium of organic-electrolyte mixtures in aerosol particles, *AIChE J.*, *48*, 1331–1348.

Quinn, P. K., and T. S. Bates (2005), Regional aerosol properties: Comparisons of boundary layer measurements from ACE 1, ACE 2, Aerosols99, INDOEX, ACE Asia, TARFOX, and NEAQS, *J. Geophys. Res.*, *110*, D14202, doi:10.1029/2004JD004755.

Quinn, P. K., and D. J. Coffman (1998), Local closure during the First Aerosol Characterization Experiment (ACE 1): Aerosol mass concentration and scattering and backscattering coefficients, *J. Geophys. Res.*, *103*(D13), 16,575–16,596.

Quinn, P. K., D. J. Coffman, V. N. Kapustin, T. S. Bates, and D. S. Covert (1998), Aerosol optical properties in the MBL during ACE-1 and the underlying chemical and physical aerosol properties, *J. Geophys. Res.*, *103*, 16,547–16,564.

Quinn, P. K., T. S. Bates, D. J. Coffman, T. L. Miller, J. E. Johnson, D. S. Covert, J.-P. Putaud, C. Neusüss, and T. Novakov (2000), A comparison of aerosol chemical and optical properties from the 1st and 2nd Aerosol Characterization Experiments, *Tellus, Ser. B*, *52*(2), 239–257, doi:10.1034/j.1600-0889.2000.00033.

Quinn, P. K., D. J. Coffman, T. S. Bates, T. L. Miller, J. E. Johnson, E. J. Welton, C. Neusüss, M. Miller, and P. J. Sheridan (2002), Aerosol optical properties during INDOEX 1999: Means, variability, and controlling factors, *J. Geophys. Res.*, *107*(D19), 8020, doi:10.1029/2000JD000037.

Quinn, P. K., et al. (2004), Aerosol optical properties measured on board the Ronald H. Brown during ACE-Asia as a function of aerosol chemical composition and source region, *J. Geophys. Res.*, *109*, D19S01, doi:10.1029/2003JD004010.

Quinn, P. K., et al. (2006), Impacts of sources and aging on submicrometer aerosol properties in the marine boundary layer across the Gulf of Maine, *J. Geophys. Res.*, doi:10.1029/2006JD007582, in press.

Remer, L. A., et al. (2005), The MODIS aerosol algorithm, products, and validation, *J. Atmos. Sci.*, *62*(4), 947–973.

Stelson, A. W. (1990), Urban aerosol refractive index prediction by partial molar refraction approach, *Environ. Sci. Technol.*, *24*, 1676–1679.

Stohl, A., M. Hittenberger, and G. Wotawa (1998), Validation of the Lagrangian particle dispersion model FLEXPART against large scale tracer experiments, *Atmos. Environ.*, *32*, 4245–4264.

Stohl, A., S. Eckhardt, C. Forster, P. James, N. Spichtinger, and P. Seibert (2002), A replacement of simple back trajectory calculations in the interpretation of atmospheric trace substance measurements, *Atmos. Environ.*, *36*, 4635–4648.

Stohl, A., O. R. Cooper, R. Damoah, F. C. Fehsenfeld, C. Forster, E. Y. Hsie, G. Huebler, D. D. Parrish, and M. Trainer (2004), Forecasting for a Lagrangian aircraft campaign, *Atmos. Chem. Phys.*, *4*, 1113–1124.

Tanré, D., Y. J. Kaufman, M. Herman, and S. Mattoo (1997), Remote sensing of aerosol properties over oceans using the MODIS/EOS spectral radiances, *J. Geophys. Res.*, *102*(D14), 16,971–16,988.

Tanré, D., F. M. Breon, J. L. Deuze, M. Herman, P. Goloub, F. Nadal, and A. Marchand (2001), Global observations of anthropogenic aerosols from satellite, *Geophys. Res. Lett.*, *28*(24), 4555–4558.

Virkkula, A., N. C. Ahlquist, D. S. Covert, W. P. Arnott, P. J. Sheridan, P. K. Quinn, and D. J. Coffman (2005), Modification, calibration and a field test of an instrument for measuring light absorption by particles, *Aerosol Sci. Technol.*, *39*(1), 68–83.

————————————

T. S. Bates, D. J. Coffman, and P. K. Quinn, Pacific Marine Environmental Laboratory, NOAA, 7600 Sand Point Way NE, Seattle, WA 98115-6349, USA. (tim.bates@noaa.gov; derek.coffman@noaa.gov; patricia.k.quinn@noaa.gov)

D. S. Covert, Joint Institute for the Study of the Atmosphere and Ocean, University of Washington, Lisa Li Building, 4909 25th Avenue NE, Box 354235, Seattle, WA 98195, USA. (dcovert@atmos.washington.edu)

B. Sierau, Department of Atmospheric Sciences, University of Washington, 408 ATG Building, Box 351640, Seattle, WA 98195-1640, USA. (bsierau@atmos.washington.edu)